Rate-Splitting for Intelligent Reflecting Surface-Assisted CR-NOMA Systems

Haoyu You, Zhiquan Bai, Hongwu Liu, Theodoros A. Tsiftsis, and Kyung Sup Kwak

***Abstract*—Intelligent reflecting surface (IRS) has been regarded as promising technique to improve system performance for wireless communications. In this paper, we propose a rate-splitting (RS) scheme for an IRS-assisted cognitive radio-inspired non-orthogonal multiple access (CR-NOMA) system, where the primary user's (PU's) quality of service (QoS) requirements must be guaranteed to be same as in orthogonal multiple access. Assisted by IRS, the threshold for the PU's tolerable interference power is improved, which in turn makes it possible to increase the achievable rate for the secondary user (SU). The optimal transmit power allocation, target rate allocation, and successive interference cancellation (SIC) decoding order are jointly designed for the proposed RS scheme. Taking into account the statistics of the direct link and IRS reflecting channels, closed-form expression for the PU's and SU's outage probabilities are respectively derived. Various simulation results are presented to clarify the enhanced outage performance achieved by the proposed RS scheme over the existing CR-NOMA and IRS-assisted CR-NOMA schemes.**

***Index Terms*—Intelligent reflecting surface, non-orthogonal multiple access, outage probability, rate-splitting.**

I. Introduction

With exponential growth of wireless data traffic demanded by Industry 4.0 networks and service-based wireless applications, available spectrum was becoming increasingly scarce [1]. As a promising multiple access solution, non-orthogonal multiple access (NOMA) has attracted great attentions from industry and academia [2]–[6]. From the point of view of cognitive radio (CR), the paired NOMA users can be deemed as a primary user (PU) and a secondary user (SU), respectively [7]. Thus, the CR principles were applied in the optimizations of transmit power allocation and successive interference cancellation (SIC) for CR-inspired NOMA (CR-NOMA) systems [8]–[11].

As a promising technology to boost the system performance for wireless communications, intelligent reflecting surface (IRS) has gained a lot of attention [12]–[15]. In general, an IRS consists of a large number of low-cost reflecting elements and can reconfigure wireless environment by reflecting beamforming. In recent years, research results have indicated that IRS-assisted NOMA was an effective solution to realize massive multiple access [16]–[19]. In many scenarios, IRS was applied to achieve superior spectral efficiency (SE) and user fairness for NOMA systems [20]–[24]. For example, IRS was proposed to maximize the sum rate for uplink NOMA systems subject to individual power constraints [20]. In [21], an energy-efficient algorithm was proposed to yield a good trade-off between the sum-rate maximization and total power consumption minimization. In [22], the authors studied the hardware architecture of the IRS and the competitive advantages of the new signal model over the existing technologies. In [23], IRS was applied in a covert communication scenario, in which a legitimate NOMA transmitter communicates with a public user aided by an IRS. In [24], a resource allocation method was proposed to achieve a higher energy efficiency for IRS-assisted systems.

In NOMA systems, multiple users may experience severe inter-user interference (IUI) if they occupy the same resource block simultaneously. In general, SIC is applied at a NOMA receiver to recover the desired signal and SIC decoding order is crucial to improve the decoding performance [25]–[28]. In [25], an SIC switching scheme was proposed to determine the SIC decoding order dynamically according to the ratio of the instantaneous received power to the target data rate of each user. In [26], a transmit power allocation scheme was proposed for the legitimate user to mitigate the error propagation caused by imperfect SIC. For CR-NOMA systems, a quality of service (QoS)-based SIC (QoS-SIC) was proposed to improve the outage performance of the SU, while the PU's outage performance was guaranteed to be same as in orthogonal multiple access (OMA) [9], [10]. Taking into SIC decoding order and power control together, a new hybrid SIC (NH-SIC) was further proposed for CR-NOMA systems to improve the SU's outage performance [11].

Due to the capability to improve spectrum efficiency, enhance reliability, and reduce latency for multi-user transmissions, rate-splitting (RS) has received a lot of attention [29], [30]. For downlink multi-user transmissions, the user messages were split into the common and private streams by using RS, which not only bridges NOMA and space

Manuscript received March 30, 2022 revised August 10, 2022; approved for publication by Yajun Zhao, Guest Editor, November 7, 2022.

This work was supported in part by National Natural Science Foundation of China under Grant 62071202, in part by Shandong Provincial Natural Science Foundation under Grant ZR2020MF009, in part by the Innovation and Development Joint Fund of Shandong Provincial Natural Science Foundation under Grant ZR2021LZH003, and in part by National Research Foundation of Korea-Grant funded by the Korean Government (MSIT)-NRF-2020R1A2B5B02002478.

H. You and H. Liu are with the School of Information Science and Electrical Engineering, Shandong Jiaotong University, Jinan 250357, China, email: 931226873@qq.com, liuhongwu@sdjtu.edu.cn.

Z. Bai is with the School of Information Science and Engineering, Shandong University, Qingdao 266237, China, email: zqbai@sdu.edu.cn.

T. A. Tsiftsis is with the School of Intelligent Systems Science and Engineering, Jinan University, Zhuhai 519070, China, email: theo_tsiftsis@jnu.edu.cn.

K. S. Kwak is with the Department of Information and Communication Engineering, Inha University, Incheon, 22212, Korea, email: kskwak@inha.ac.kr.

H. Liu is the corresponding author.

Digital Object Identifier: 10.23919/JCN.2022.000053

1229-2370/22/$10.00 © 2022 KICS

division multiple access (SDMA), but also provides trade-off between system performance and implementation complexity [31]. Different from RS-aided downlink transmissions, data streams transmitted by all users are fully decoded at the base-station (BS) using SIC in RS-aided uplink transmissions [32]–[35]. Subject to individual rate constraints, RS was applied to maximize the sum-rate for uplink rate-splitting multiple access (RSMA) systems [32]. In single-input multiple-output (SIMO) NOMA systems, RS was used to ensure maximum-minimum fairness among uplink users [35]. To avoid exhaustive search in the determination of the optimal SIC decoding order required by uplink RSMA, the fixed RS and cognitive RS schemes were proposed for CR-NOMA systems with the increased outage performance and user fairness [36]. Recently, a CR-inspired RS scheme incorporating the transmit power allocation and SIC decoding order was proposed for CR-NOMA systems to improve the SU's outage performance [37]. Further, the CR-inspired RS scheme was applied to enhance the computation performance in mobile edge computing systems [38].

In this paper, we propose to use RS to improve the outage performance of an IRS-assisted CR-NOMA (IRS-CR-NOMA) system. The transmissions from PU to BS are assisted by an IRS, which improves the equivalent channel gain from PU to BS and results in an improved tolerable interference power threshold for PU. Without deteriorating the PU's outage performance, RS is conducted the SU to improve the outage performance of the SU. Benefitting from IRS and RS, the proposed scheme achieves a superior outage performance than the benchmark schemes in which the IRS and RS are not deployed.

The main contributions of this paper are summarized as follows:

- For the considered CR-NOMA system, we apply the IRS to assist the PU's transmission and attain an improved tolerable interference power threshold. Then, we apply a RS scheme to improve the outage performance of the SU. For the RS scheme, the optimal transmit power allocation, target rate allocation, and SIC decoding order are jointly designed.
- Taking into account the IRS-assisted channel gain, we derive the closed-form expression for the outage probability of the SU, which significantly facilitates the evaluation of the outage performance. The impact of target rate and transmit power allocation on the SU's outage performance is revealed. Various simulation results are presented to clarify the enhanced outage performance achieved by the proposed scheme than the existing benchmark schemes in which the IRS and RS are not deployed.

The remainder of this paper is organized as follows: In Section II, the system model of the IRS-CR-NOMA system is presented. In Section III, we present the RS scheme and provide the outage performance analysis. In Section IV, simulation results are presented to verify the enhanced outage performance achieved by the proposed scheme. Section V summarizes this work.

Notation: The cumulative distribution function (CDF) and probability density function (PDF) of the random variable (RV) x are denoted by $F_x(\cdot)$ and $f_x(\cdot)$, respectively. $\Gamma(m,n) = \int_n^\infty t^{m-1}\exp(-t)\,dt$ and $\gamma(m,n) = \int_0^n t^{m-1}\exp(-t)\,dt$ denote the upper incomplete Gamma function and lower incomplete gamma function, respectively. $\Gamma(x) = \int_0^\infty t^{x-1}\exp(-t)\,dt$ denotes the Gamma function. $[\boldsymbol{a}]_n$ and $[\boldsymbol{A}]_n$ denote the nth element of the vector $\boldsymbol{a}$ and matrix $\boldsymbol{A}$, respectively. $\mathrm{diag}(\boldsymbol{a})$ means generating a diagonal matrix using the elements of the vector $\boldsymbol{a}$. $(\cdot)^H$ and $(\cdot)^T$ denote Hermitian transpose and transpose, respectively. An identity matrix of the size $N \times N$ is denoted by I_N. $\mathbb{E}(\cdot)$ and $\mathrm{Var}(\cdot)$ means the expectation and variance of a RV, respectively.

II. System Model

We consider an uplink CR-NOMA system consisting of a PU U_1, a SU U_2, and a BS, as depicted in Fig. 1. To assist the PU's transmission, an IRS is deployed between the BS and PU, so that the PU can transmit its signal to the BS via the direct link and the IRS-reflected channels. We assume that the SU is located in a position without IRS being available in its vicinity. To facilitate the outage performance analysis, we assume that each node is equipped with a single antenna for transmission/reception, while the IRS consists of N reflecting elements.

In the considered system, the direct link channel from U_i $(i = 1, 2)$ to the BS is denoted by $\tilde{h}_i = \sqrt{L_i}h_i$, where L_i is the distance-related path-loss and h_i is the small-scale fading coefficient. The reflecting channels from U_1 to IRS and from IRS to BS are denoted by $\tilde{\boldsymbol{h}}_{\mathrm{UI}} = \sqrt{L_{\mathrm{UI}}}\boldsymbol{h}_{\mathrm{UI}}$ and $\tilde{\boldsymbol{h}}_{\mathrm{IB}} = \sqrt{L_{\mathrm{IB}}}\boldsymbol{h}_{\mathrm{IB}}$, respectively, where $\boldsymbol{h}_{\mathrm{UI}}$ and $\boldsymbol{h}_{\mathrm{IB}}$ are the $N \times 1$ vectors containing the small-scale fading coefficients, L_{UI} and L_{IB} are the distance-related path-loss associated with the reflecting channels. In this paper, we assume that all the small-scale fading coefficients follow independent and identically distributed Rayleigh fading and model the large-scale fading by using the distance-related path-loss, which is given by

$$L_i = \left(\frac{d_i}{d_0}\right)^{-\chi}, \tag{1}$$

where $d_i \in \{d_1, d_2, d_{\mathrm{UI}}, d_{\mathrm{IB}}\}$ denotes the distance associated with the corresponding channel, d_0 denotes the reference distance, and χ is the path-loss exponential component.

For the IRS, we assume the unit reflecting amplitude for each element and use $\phi_n \in (-\pi, \pi]$ to denote the reflecting phase-shift generated by the nth element $(n = 1, 2, \cdots, N)$. To attain the strongest channel gain for the PU's transmission, the ideal phase-shift is adopted as $\phi_n = \arg(h_1) - \arg([\boldsymbol{h}_{\mathrm{IB}}]_n[\boldsymbol{h}_{\mathrm{UI}}]_n)$, where $[\boldsymbol{h}_{\mathrm{IB}}]_n$ and $[\boldsymbol{h}_{\mathrm{UI}}]_n$ are the nth elements of h_{IB} and h_{IB}, respectively. Then, the phase-shift matrix of the IRS can expressed as $\boldsymbol{Q} = \mathrm{diag}\left(\left[e^{j\phi_1}, e^{j\phi_2}, \cdots e^{j\phi_N}\right]\right)$. For the PU's transmission to the BS, the equivalent channel gain can be written as:

$$g_1 = \left|\sqrt{L_1}h_1 + \sqrt{L_R}\boldsymbol{h}_{\mathrm{IB}}^H\boldsymbol{Q}\boldsymbol{h}_{\mathrm{UI}}\right|^2, \tag{2}$$

where $L_R = \left(d_{\mathrm{IB}}d_{\mathrm{UI}}/d_0^2\right)^{-\chi}$ is the distance-related path-loss of the reflecting channels.

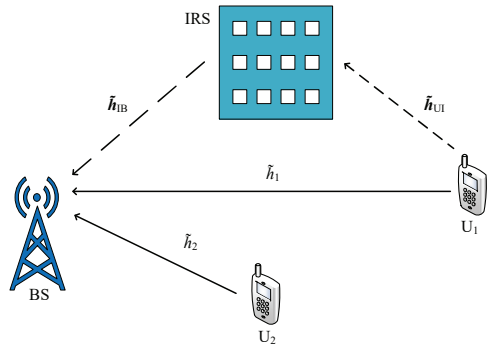

Fig. 1. System model.

Prior to transmission, the BS sends an interference power threshold τ to the SU with the aim of guaranteeing the QoS requirements of the PU. The interference power threshold is given by [10], [11]

$$\tau = \max\left\{0, \frac{P_1 g_1}{\varepsilon_1} - \sigma^2\right\}, \tag{3}$$

where P_i is the transmit power of U_i, σ^2 is the variance of the additive white Gaussian noise (AWGN) the BS receiver, and $\varepsilon_1 = 2^{\hat{R}_1} - 1$ with $\hat{R}_1$ denoting the target rate of U_1. Since the maximum value of g_1 can be achieved by using the ideal phase-shift, an increased interference power threshold is attained by using the IRS to assist the PU's transmissions.

To improve the outage performance of the considered CR-NOMA system, not only the IRS is deployed between the BS and PU, but also the RS is conducted at the SU. Since $2K-1$ split data streams are enough to approach the full capacity region for the uplink RSMA containing K users [39], we only consider RS at the SU, equivalently, the PU does not need to perform RS.

For each transmission block, the message signal of the SU can be split into two parts x_{21} and x_{22} to be transmitted. The signal received at the BS can be expressed as:

$$\begin{aligned} y = &\left(\sqrt{L_1}h_1 + \sqrt{L_R}\boldsymbol{h}_{\mathrm{IB}}^H \boldsymbol{Q} \boldsymbol{h}_{\mathrm{UI}}\right)\sqrt{P_1}x_1 + \sqrt{\alpha P_2 L_2}h_2 x_{21} \\ &+\sqrt{(1-\alpha)P_2 L_2}h_2 x_{22} + n, \end{aligned} \tag{4}$$

where P_2 is the transmit power of U_2, n is the AWGN at the BS with zero mean and variance σ^2 and α is the transmit power allocation factor satisfying $0 \le \alpha \le 1$.

To attain the maximum achievable rate for the SU, the SIC decoding order $x_{21} \to x_1 \to x_{22}$ is used at the BS receiver [37], [39]. Then, for the detections of x_{21}, x_1, and x_{22}, the received signal-to-noise ratios (SNRs) can be expressed as:

$$\gamma_{21} = \frac{\alpha\rho_2 g_2}{(1-\alpha)\rho_2 g_2 + \rho_1 g_1 + 1}, \tag{5}$$

$$\gamma_1 = \frac{\rho_1 g_1}{(1-\alpha)\,\rho_2 g_2 + 1}, \tag{6}$$

and

$$\gamma_{22} = (1-\alpha)\rho_2 g_2, \tag{7}$$

respectively, where $\rho_1 = P_1 g_1/\sigma^2$ and $\rho_2 = P_2 g_2/\sigma^2$ with $g_2 = L_2|h_2|^2$. For the transmissions of x_{21}, x_1, and x_{22}, the achievable rates are then given by $R_{21} = \log_2(1+\gamma_{21})$, $R_1 = \log_2(1+\gamma_1)$, and $R_{22} = \log_2(1+\gamma_{22})$, respectively.

For the considered system, the RS is deigned to obtain the allowed maximum achievable rate for the SU, which in turn can improve the SU's outage performance. Corresponding to the SIC decoding order $x_{21} \to x_1 \to x_{22}$, the RS operations at the SU are determined by comparing the SU's channel gain to the interference power threshold, which are categorized as the following three cases:

1) Case I: $\tau > 0$ and $\rho_2 g_2 \le \tau$. In this case, the maximum interference power resulted by the SU's transmission of x_{22} is no more than the interference power threshold. Thus, the SU does not conduct RS and allocates all of P_2 to transmit x_2 ($x_{22} = x_2$), where x_2 is the transmit signal generated by U_2 from to its message signal without conducting RS. Consequently, the transmit power allocation is set as $\alpha = 0$ and the SIC decoding order $x_{21} \to x_1 \to x_{22}$ degrades to $x_1 \to x_2$ (or equivalently $x_1 \to x_{22}$) the BS receiver. In this case, the received SNR for decoding x_1 and x_2 are given by $\gamma_1 = \frac{\rho_1 g_1}{\rho_2 g_2 + 1}$ and $\gamma_2 = \rho_2 g_2$, respectively, and the achievable rate for the SU is given by $R_2^{(\mathrm{I})} = \log_2(1+\rho_2 g_2)$.

2) Case II: $\tau > 0$ and $\rho_2 g_2 > \tau$. In this case, in order to attain the allowed maximum achievable rate for the SU, U_2 applies RS by setting $\alpha = 1 - \frac{\tau}{\rho_2 g_2}$, which results in the achievable rates $R_{21} = \log_2(1 + \frac{\rho_2 g_2 - \tau}{\rho_1 g_1 + \tau + 1})$ and $R_{22} = \log_2(1+\tau)$. Since R_{22} achieves the maximum value allowed by the interference power threshold, the achievable rate $R_2^{(\mathrm{II})} = R_{21} + R_{22}$ of the SU is maximized in this case, which is given by $R_2^{(\mathrm{II})} = \log_2(1 + \frac{\rho_2 g_2 - \tau}{\rho_1 g_1 + \tau + 1}) + \log_2(1+\tau)$. Corresponding to the transmissions of x_{21} and x_{22}, the target rate $\hat{R}_2$ of U_2 is split into $\hat{R}_{21}$ and $\hat{R}_{22}$, respectively. To ensure the successful detection of x_{22}, the split target rate is given by $\hat{R}_{22} = R_{22} = \log_2(1+\tau)$. Then, the split target rate $\hat{R}_{21} = \hat{R}_2 - \hat{R}_{22}$ is set for the transmission of x_{21}. To avoid error propagation in SIC, it requires the successful detection of x_{21} in the first stage of the SIC decoding order $x_{21} \to x_1 \to x_{22}$. Thus, the transmission of the SU only occurs if $R_{21} \ge \hat{R}_{21}$. Otherwise, the SU keeps silence, while the PU transmit alone in this case.

3) Case III: $\tau = 0$. In this case, the PU's transmission encounters an outage due to a weak channel gain g_1. Thus, U_2 does not conduct RS and transmits the signal $x_{21} = x_2$ by setting $\alpha = 1$. Consequently, the SIC decoding order at the BS degrades to $x_2 \to x_1$ (or equivalently $x_{21} \to x_1$). The achievable rate of the SU is given by $R_2^{(\mathrm{III})} = \log_2(1 + \frac{\rho_2 g_2}{\rho_1 g_1 + 1})$.

Assisted by the IRS, the interference power threshold τ is improved the achievable rate of U_2 attained by the proposed RS scheme can be expressed as follows:

$$R_2 = \begin{cases} R_2^{(\mathrm{I})}, & \tau > 0 \ \text{ and } \ \rho_2 g_2 \le \tau \\ R_2^{(\mathrm{II})}, & \tau > 0 \ \text{ and } \ \rho_2 g_2 > \tau \\ R_2^{(\mathrm{III})}, & \tau = 0. \end{cases} \tag{8}$$

Corresponding to Cases I, II, and III, the achievable rates of U_1 can be characterized by $R_1 = \log_2\left(1 + \frac{\rho_1 g_1}{\rho_2 g_2 + 1}\right)$, $R_1 \ge \log_2\left(1 + \frac{\rho_1 g_1}{\tau + 1}\right)$, and $R_1 \le \log_2(1+\rho_1 g_1)$, respectively.

Compared to the CR-NOMA system, the deployment of the IRS can increase the equivalent channel gain g_1 in the considered IRS-CR-NOMA system, which is beneficial to improve the PU's outage probability. On the other hand, the IRS-CR-NOMA scheme generated an increased τ, corresponding to which the SU has a higher probability to operate in Cases I and II. Thus, a higher achievable rate can be attained by the SU with the aid of IRS and RS, which in turn will improve the outage performance of the SU.

III. Outage Performance Analysis

In this section, we analyze the outage performance for the PU and SU achieved by the RS scheme in the considered IRS-CR-NOMA system. First, the distributions of the involved channel gains are derived. Then, the closed-form expressions for the outage probabilities of the PU and SU are presented, respectively. Asymptotic approximations are also discussed for the outage probabilities of the PU and SU in the high SNR region.

A. Channel Gain Distribution Analysis

For the PU's transmission, the equivalent channel gain g_1 is given by (2). Substituting the ideal phase-shift into (2), g_1 can be rewritten as:

$$g_1 = \left| \sqrt{L_1}|h_1| + \sqrt{L_R}\sum_{n=1}^{N} |[\boldsymbol{h}_{\mathrm{IB}}]_n||[\boldsymbol{h}_{\mathrm{UI}}]_n| \right|^2. \tag{9}$$

The CDF of g_1 is $F_{g_1}(z) = \Pr(g_1 < z)$, which has an analytical expression given in the following Theorem.

Theorem 1: The CDF of the equivalent channel gain g_1 is given by

$$F_{g_1}(z) = 1 - \Gamma(k, \sqrt{z}/\theta)/\Gamma(k), \tag{10}$$

where k and θ denote the shape and scale parameters of Gamma distribution, respectively, which are given by

$$k = \frac{\left(\sqrt{L_1\pi} + 2N\xi\psi\right)^2}{4L_1 + 4N\xi\psi^2 - L_1\pi}, \tag{11}$$

and

$$\theta = \frac{4L_1 + 4N\xi\psi^2 - L_1\pi}{2\left(\sqrt{L_1\pi} + 2N\xi\psi\right)}, \tag{12}$$

respectively, with $\xi = \frac{\pi^2}{16-\pi^2}$ and $\psi = \left(4 - \frac{\pi^2}{4}\right)\sqrt{L_{\mathrm{IB}}L_{\mathrm{UI}}}\pi$.

Proof: See Appendix A. ∎

The results in Theorem 1 gives a closed-form expression for the CDF of g_1 in terms of the large-scale fading coefficients, which is beneficial to evaluate the outage performance.

The CDF of g_1 in (10) can be further rewritten as:

$$\begin{aligned} F_{g_1}(z) &= \frac{1}{\Gamma(k)}\gamma(k, \sqrt{z}/\theta) \\ &= \frac{1}{\theta^k\Gamma(k)}\sum_{m=0}^{\infty}\left(-\frac{1}{\theta}\right)^m \frac{z^{\frac{m+k}{2}}}{m!(m+k)}. \end{aligned} \tag{13}$$

In the high SNR region as $\rho \to \infty$, the CDF of g_1 can be approximated as:

$$F_{g_1}(z) = \frac{z^{\frac{k}{2}}}{k\theta^k\Gamma(k)}. \tag{14}$$

With the above approximated CDF, the PDF of g_1 can be evaluated as:

$$f_{g_1}(z) = \frac{z^{\frac{k}{2}-1}}{2\theta^k\Gamma(k)}. \tag{15}$$

For the SU's transmission, since the direct link channel gain g_2 is an exponential RV, the CDF of g_2 can be written as:

$$F_{g_2}(z) = 1 - e^{-\frac{z}{L_2}}. \tag{16}$$

B. Outage Probability Analysis

In this subsection, the outage probabilities of the PU and SU achieved by the proposed RS scheme in the IRS-CR-NOMA system are respectively derived.

For the PU, the outage probability is given by $P_{\mathrm{out},1} = \Pr(R_1 < \hat{R}_1)$, which can be further evaluated as:

$$\begin{aligned} P_{\mathrm{out},1} &= \Pr(\tau = 0) \\ &= \Pr(g_1 \le \eta_1) \\ &= 1 - \Gamma(k, \sqrt{\eta_1}/\theta)/\Gamma(k), \end{aligned} \tag{17}$$

where $\eta_1 = \varepsilon_1/\rho_1$.

For the SU, the outage probability can be expressed as:

$$P_{\mathrm{out},2} = P_{\mathrm{out},2}^{(\mathrm{I})} + P_{\mathrm{out},2}^{(\mathrm{II})} + P_{\mathrm{out},2}^{(\mathrm{III})}, \tag{18}$$

where $P_{\mathrm{out},2}^{(\mathrm{I})} = \Pr\{\tau > 0, \rho_2 g_2 \le \tau, R^{(\mathrm{I})} < \hat{R}_2\}$, $P_{\mathrm{out},2}^{(\mathrm{II})} = \Pr\{\tau > 0, \rho_2 g_2 > \tau, R^{(\mathrm{II})} < \hat{R}_2\}$ and $P_{\mathrm{out},2}^{(\mathrm{III})} = \Pr\{\tau = 0, R^{(\mathrm{III})} < \hat{R}_2\}$ indicate the probabilities that U_2 is outage corresponding to Cases I, II, and III, respectively. The Closed-form expressions for $P_{\mathrm{out}}^{(\mathrm{I})}$, $P_{\mathrm{out}}^{(\mathrm{II})}$, and $P_{\mathrm{out}}^{(\mathrm{III})}$ are provided in the following propositions, respectively.

Proposition 1: Corresponding to the RS scheme's operation in Case II, the probability $P_{\mathrm{out}}^{(\mathrm{II})}$ is given by

$$P_{\mathrm{out},2}^{(\mathrm{II})} = I_1 - I_2, \tag{19}$$

where I_1 and I_2 are given by (20) and (21), respectively, as shown on the top of the next page.

Proof: See Appendix B. ∎

Proposition 2: Corresponding to the RS scheme's operations in Case I and Case III, the probabilities $P_{\mathrm{out},2}^{(\mathrm{I})}$ and $P_{\mathrm{out},2}^{(\mathrm{III})}$ are given by

$$\begin{aligned} P_{\mathrm{out},2}^{(\mathrm{I})} &= F_{g_1}(\eta_1(1+\varepsilon_2))(1 - F_{g_2}(\eta_2)) + F_{g_2}(\eta_2) \\ &\quad - F_{g_1}(\eta_1) - I_3, \end{aligned} \tag{22}$$

and

$$P_{\mathrm{out},2}^{(\mathrm{III})} = F_{g_1}(\eta_1) - I_4, \tag{23}$$

where I_3 and I_4 are given by

$$I_3 = \frac{(\rho_2 L_2\eta_1)^{\frac{k}{2}} e^{\frac{1}{\rho_2 L_2}}}{2\theta^k\Gamma(k)}\left(\gamma\left(\frac{k}{2}, \frac{1+\varepsilon_2}{\rho_2 L_2}\right) - \gamma\left(\frac{k}{2}, \frac{1}{\rho_2 L_2}\right)\right),$$

$$I_1 = \frac{e^{\frac{1}{\rho_2 L_2}}}{2\theta^k \Gamma(k)} \left(\frac{\rho_2 \varepsilon_1 L_2}{\rho_1}\right)^{\frac{k}{2}} \left(\gamma\left(\frac{k}{2}, \frac{1+\varepsilon_2}{\rho_2 L_2}\right) - \gamma\left(\frac{k}{2}, \frac{1}{\rho_2 L_2}\right)\right), \tag{20}$$

$$I_2 = \frac{e^{-\frac{\varepsilon_1+\varepsilon_2+\varepsilon_1\varepsilon_2}{\rho_2 L_2}}}{2\theta^k \Gamma(k)} \left(-\frac{\rho_2 L_2}{\rho_1}\right)^{\frac{k}{2}} \left(\gamma\left(\frac{k}{2}, -\frac{\rho_1\eta_1}{\rho_2 L_2}\right) - \gamma\left(\frac{k}{2}, -\frac{\rho_1\eta_1(1+\varepsilon_2)}{\rho_2 L_2}\right)\right). \tag{21}$$

(24)

and

$$I_4 = \frac{e^{-\frac{\varepsilon_2}{\rho_2 L_2}}}{2\theta^k \Gamma(k)} \left(\frac{\rho_2 L_2}{\rho_1 \varepsilon_2}\right)^{\frac{k}{2}} \gamma\left(\frac{k}{2}, \frac{\varepsilon_1\varepsilon_2}{\rho_2 L_2}\right), \tag{25}$$

respectively.

Proof: See Appendix C. ■

By combing (19), (22), and (23) together, the outage probability experienced by the U_2 in the proposed RS scheme is given by

$$\begin{aligned} P_{\text{out},2} &= F_{g_1}(\eta_1(1+\varepsilon_2))(1 - F_{g_2}(\eta_2)) + F_{g_2}(\eta_2) \\ &\quad + I_1 - I_2 - I_3 - I_4 \\ &= -\frac{e^{-\frac{\eta_2}{L_2}} \Gamma\left(k, \frac{\sqrt{\eta_1(1+\varepsilon_2)}}{\theta}\right)}{\Gamma(k)} + I_1 - I_2 - I_3 - I_4. \end{aligned} \tag{26}$$

Remark 1: We demonstrate by the following examples that the proposed RS scheme can achieve higher achievable rate than the IRS-CR-NOMA scheme which does not deploy the RS.

Example 1: $\log_2(1+\tau) > \log_2\left(1 + \frac{\rho_2 g_2}{\rho_1 g_1 + 1}\right)$. In this example, we assume $g_1 = g_2 = 15$, $\rho_1 = 15$, $\rho_2 = 25$, and $\varepsilon_1 = 4$. The interference threshold is give by $\tau = \frac{225}{4}$. For the IRS-CR-NOMA scheme without RS, the achievable rate of U_2 is $R_2^{(\text{II})} = \log_2\left(1 + \frac{625}{226}\right) \approx 0.58$ BPCU. In contrast, the proposed scheme achieves $R_2^{(\text{II})} = \log_2\left(1 + \frac{318.75}{282.25}\right) + \log_2\left(1 + \frac{225}{4}\right) \approx 2.09$ BPCU.

Example 2: $\log_2(1+\tau) < \log_2\left(1 + \frac{\rho_2 g_2}{\rho_1 g_1 + 1}\right)$. In this example, we assume $g_1 = g_2 = 10$, $\rho_1 = 1$, $\rho_2 = 20$, and $\varepsilon_1 = 3$. The interference threshold is give by $\tau = \frac{7}{3}$. For the IRS-CR-NOMA scheme without RS, the achievable rate of U_2 is $R_2^{(\text{II})} = \log_2\left(1 + \frac{200}{11}\right) \approx 4.26$ BPCU. In contrast, the proposed scheme achieves $R_2^{(\text{II})} = \log_2\left(1 + \frac{593}{40}\right) + \log_2\left(1 + \frac{7}{3}\right) \approx 5.72$ BPCU.

IV. Simulation Results

In this section, we present the numerical results to clarify the outage performance achieved by the proposed RS scheme and verify the accuracy of the developed analytical expressions. For comparison purpose, we also present the simulation results of the CR-NOMA and IRS-CR-NOMA schemes. Unless otherwise specified, the following parameters are used throughout the simulation: $\sigma^2 = 10^{-8}$ W, $N = 32$, $\chi = 3$, $d_0 = 1$ m, $d_1 = 17$ m, $d_2 = 15$ m, $d_{\text{UI}} = 10$ m, $d_{\text{IB}} = 8$ m.

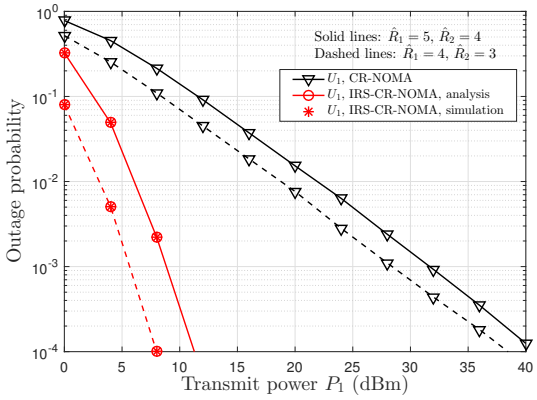

Fig. 2. The PU's outage probability comparison.

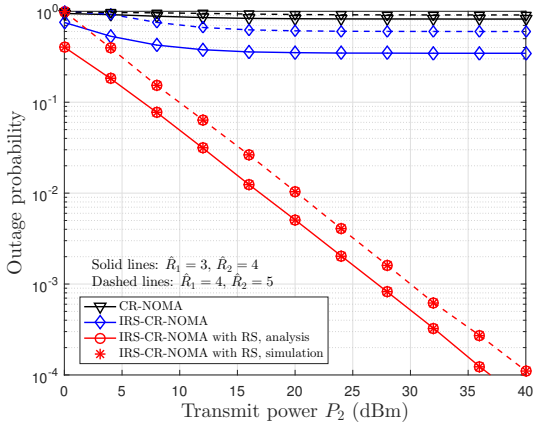

Fig. 3. The SU's outage probability comparison.

In Fig. 2, the outage probability of U_1 achieved by the IRS-CR-NOMA scheme is compared with the CR-NOMA scheme for various transmit power settings, where we set $P_1 = P_2$ and $N = 8$, respectively. In particular, we consider two target rate settings $\{\hat{R}_1 = 5\,\text{BPCU}, \hat{R}_2 = 4\,\text{BPCU}\}$ and $\{\hat{R}_1 = 4\,\text{BPCU}, \hat{R}_2 = 3\,\text{BPCU}\}$ in Fig. 2. We can see from Fig. 2, the outage probabilities of U_1 achieved by the IRS-CR-NOMA and CR-NOMA schemes monotonically decrease with an increasing of transmit power. It is clearly illustrating that the IRS-CR-NOMA scheme achieves better outage performance than CR-NOMA scheme for U_1 in the whole transmit power region, which proves that the usage of IRS is helpful to improve the outage performance of the PU.

In Fig. 3, the outage probability of U_2 achieved by the proposed RS scheme is compared with the CR-NOMA scheme and IRS-CR-NOMA schemes for various transmit

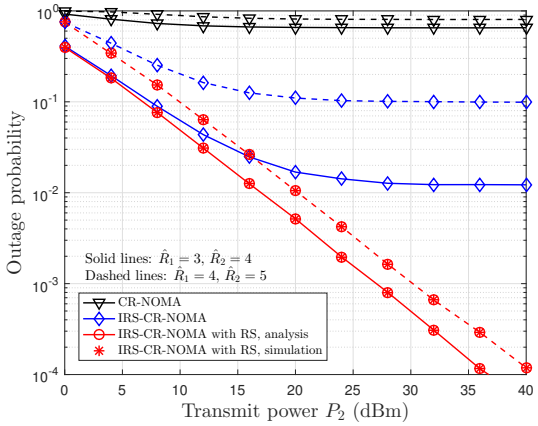

Fig. 4. Outage probability comparison for U_2 with $P_1 = 5P_2$.

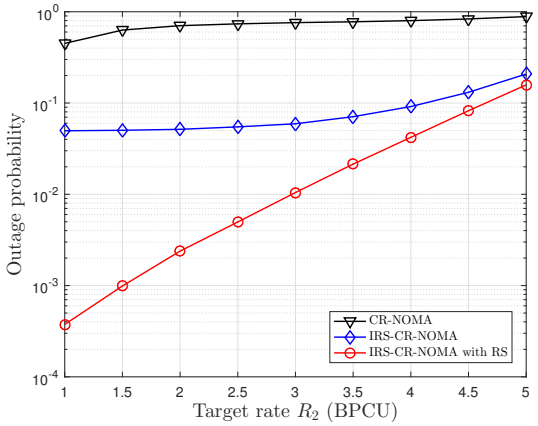

Fig. 5. Impact of the target rate on the outage probability of U_2.

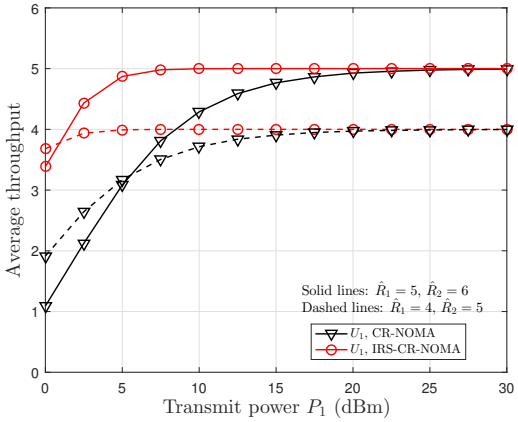

Fig. 6. Average throughput comparison for U_1.

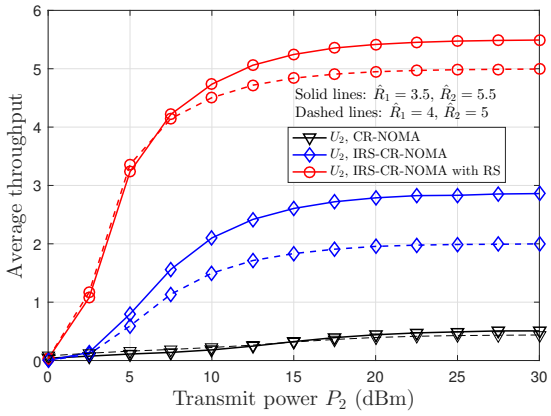

Fig. 7. Average throughput comparison for U_2.

power settings, where we set $P_1 = P_2$. In particular, we set $\{\hat{R}_1 = 3\,\text{BPCU}, \hat{R}_2 = 4\,\text{BPCU}\}$ and $\{\hat{R}_1 = 4\,\text{BPCU}, \hat{R}_2 = 5\,\text{BPCU}\}$ in Fig. 3. From Fig. 3, we can see that the proposed RS scheme achieves the best outage performance among the three schemes. In addition, we can see that the outage probability of the three schemes approach 1 in the low transmit power region. As the transmit power increases, the outage probabilities achieved by the CR-NOMA and IRS-CR-NOMA scheme encounter a outage probability floor in the middle and high SNR regions. On the contrary, we can see from Fig. 3, that the outage probability of the proposed RS scheme monotonically decreases with an increasing transmit power.

In Fig. 4, we investigate the outage performance of U_2 achieved by the considered three schemes for various transmit power settings. In particular, we set $P_1 = 5P_2$ in Fig. 4. In addition, we set $\{\hat{R}_1 = 3\,\text{BPCU}, \hat{R}_2 = 4\,\text{BPCU}\}$ and $\{\hat{R}_1 = 4\,\text{BPCU}, \hat{R}_2 = 5\,\text{BPCU}\}$ for target rate pair $\hat{R}_1$ and $\hat{R}_2$ in Fig. 4. From Fig. 4, we can see that the proposed RS scheme achieves the smaller outage probability than CR-NOMA scheme and IRS-CR-NOMA scheme for both $\{\hat{R}_1 = 3\,\text{BPCU}, \hat{R}_2 = 4\,\text{BPCU}\}$ and $\{\hat{R}_1 = 4\,\text{BPCU}, \hat{R}_2 = 5\,\text{BPCU}\}$. Furthermore, we can see from Fig. 4 that the outage probabilities of the CR-NOMA and IRS-CR-NOMA encounter an outage probability floor in the middle and high SNR regions. In contrast, the outage probability achieved by the proposed scheme (IRS-CR-NOMA with RS) monotonically decreases with an increasing of the transmit power.

In Fig. 5, the outage probability of U_2 achieved by the proposed RS scheme is compared with the CR-NOMA and IRS-CR-NOMA schemes for various settings of the target rates. In particular, we set $P_1 = 25$ dBm, $P_2 = 20$ dBm and fix the target rate $\hat{R}_1 = 3$ BPCU in Fig. 5. It is clearly illustrating that the proposed RS scheme achieves the best outage performance among the three schemes in the whole target rate region. In the low target rate region, we can see that the CR-NOMA scheme achieves the highest outage probability among the three schemes. Although the IRS-CR-NOMA scheme achieves a lower outage probability than that of the CR-NOMA scheme, the achieved outage probability is still higher than that of the proposed RS scheme in the considered target rate region.

In Fig. 6, the average throughput of U_1 achieved by the IRS-CR-NOMA scheme is compared with the CR-NOMA scheme for various transmit power settings, where we set $P_1 = P_2$ and $N = 8$. In addition, we set $\{\hat{R}_1 = 5\,\text{BPCU}, \hat{R}_2 = 6\,\text{BPCU}\}$ and $\{\hat{R}_1 = 4\,\text{BPCU}, \hat{R}_2 = 5\,\text{BPCU}\}$ in Fig. 6. From Fig. 6, we can see that the average throughputs achieved by both schemes increases monotonically with an increasing of the transmit power in the low transmit power

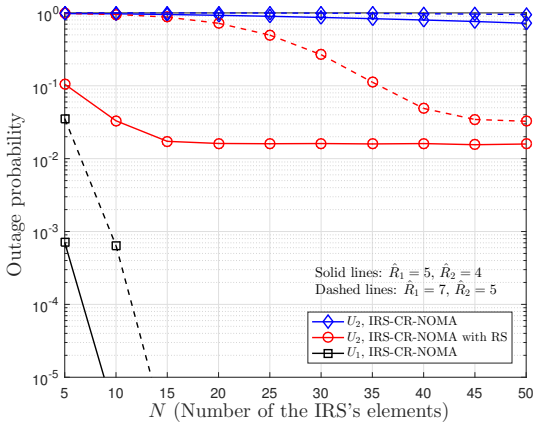

Fig. 8. Impact of the number of IRS's elements on the outage probability.

region. In the middle and high transmit power regions, the average throughputs achieved by both schemes approach the target rate, respectively. However, in the low and middle transmit power regions, the IRS-CR-NOMA scheme always achieves a higher average throughput than that of the CR-NOMA scheme, which verifies that the use of the IRS can improve the PU's average throughput.

In Fig. 7, the average throughput of U_2 achieved by the proposed RS scheme is compared with the CR-NOMA and IRS-CR-NOMA schemes for various transmit power settings, where we set $P_1 = P_2$. In particular, we assume $\{\hat{R}_1 = 3.5\,\text{BPCU}, \hat{R}_2 = 5.5\,\text{BPCU}\}$ and $\{\hat{R}_1 = 4\,\text{BPCU}, \hat{R}_2 = 5\,\text{BPCU}\}$ in Fig. 7, respectively. From Fig. 7, we can see that the proposed RS scheme achieves the best average throughputs among the three schemes for two different target rates, respectively. In addition, we can see that the average throughput of the three schemes approaches 0 in the low transmit power region. The average throughput achieved by the three schemes increases with the increasing of transmit power and stabilizes in the high transmit power region. However, only the average throughput achieved by the RS scheme approaches the target rate in the high transmit power region, whereas the average throughputs acheived by the CR-NOMA and IRS-CR-NOMA schemes are lower that the target rate in the whole transmit power region.

In Fig. 8, the impact of the number of the IRS's reflecting elements is investigated, where we set $P_1 = P_2 = 15$ dBm. In particular, we assume $\{\hat{R}_1 = 5\,\text{BPCU}, \hat{R}_2 = 4\,\text{BPCU}\}$ and $\{\hat{R}_1 = 7\,\text{BPCU}, \hat{R}_2 = 5\,\text{BPCU}\}$ in Fig. 8, respectively. From the curves in Fig. 8, we can see that the RS scheme achieves a lower outage probability for U_2 than that of the IRS-CR-NOMA without deploying the RS. With the increasing of N, the SU's outage probability achieved by the RS scheme first decreases and then approaches a outage probability floor in the middle and high N regions. The reason for this phenomenon is that the outage performance is limited by the considered fixed transmit power (15 dBm for this figure), so that the increasing of N cannot further improve the outage performance when the available best outage performance has been approached.

V. Conclusions

In this paper, we have proposed to use RS to improve the outage performance of the IRS-CR-NOMA system, in which the PU and SU communicate with a BS simultaneously. Assisted by the IRS, the PU attained an improved tolerable interference power threshold, which resulted in an improved outage performance for the PU. Under the CR principles, RS has been conducted at the RS to aid its transmission. The optimal power allocation, target allocation, and SIC decoding order have been jointly designed to attain the maximum achievable rate for the SU, meanwhile guaranteeing the PU's outage performance to be same as in OMA. The closed-form expressions for the outage probabilities of the PU and SU have been derived. Numerical results have shown that the proposed RS scheme achieved a better outage performance than the CR-NOMA and IRS-CR-NOMA schemes without deploying RS.

Appendix A: A Proof of Theorem 1

Corresponding to g_1 in (9), we define $A \triangleq \sqrt{L_1}\,|h_1|$ and $B_n \triangleq \sqrt{L_R}\,|[\boldsymbol{h}_{\text{IB}}]_n|\,|[\boldsymbol{h}_{\text{UI}}]_n|$, $\forall n$. The RV A follows Rayleigh distribution with the mean $\sqrt{L_1\pi}/2$ and variance $(4-\pi)L_1/4$. Also, $|[\boldsymbol{h}_{\text{IB}}]_n|$ and $|[\boldsymbol{h}_{\text{UI}}]_n|$ follow Rayleigh distribution and the corresponding CDF and PDF are given by

$$F_{[h_x]_n}(z) = 1 - e^{\left(-\frac{z^2}{L_x}\right)}, \tag{A.1}$$

and

$$f_{[h_x]_n}(z) = \frac{2z}{L_x} e^{\left(-\frac{z^2}{L_x}\right)}, \tag{A.2}$$

respectively, where $x \in \{\text{IB}, \text{UI}\}$. Then, the CDF of B_n can be expressed as:

$$\begin{aligned} F_{B_n}(z) &= \Pr(B_n < z) \\ &= \Pr\left(|[\boldsymbol{h}_{\text{IB}}]_n| < \frac{z}{|[\boldsymbol{h}_{\text{UI}}]_n|} = \frac{z}{t}\right) \\ &= \int_0^\infty F_{[\boldsymbol{h}_{\text{IB}}]_n}\left(\frac{z}{t}\right) f_{[\boldsymbol{h}_{\text{UI}}]_{n=t}}(t)\,dt \\ &= 1 - \frac{2z}{\sqrt{L_{\text{IB}}L_{\text{UI}}}} K_1\left(\frac{2z}{\sqrt{L_{\text{IB}}L_{\text{UI}}}}\right), \end{aligned} \tag{A.3}$$

where $K_n(\cdot)$ is the modified Bessel function of the second kind with n-th order. By using [40, Eq. (8.486.11)], the PDF of B_n can be evaluated as:

$$\begin{aligned} f_{B_n}(z) &= \frac{dF_{B_n}(z)}{dz} \\ &= \frac{2z}{L_{\text{IB}}L_{\text{UI}}}\left(K_2\left(\frac{2z}{\sqrt{L_{\text{IB}}L_{\text{UI}}}}\right) + K_0\left(\frac{2z}{\sqrt{L_{\text{IB}}L_{\text{UI}}}}\right)\right) \\ &\quad - \frac{2}{\sqrt{L_{\text{IB}}L_{\text{UI}}}} K_1\left(\frac{2z}{\sqrt{L_{\text{IB}}L_{\text{UI}}}}\right). \end{aligned} \tag{A.4}$$

By using the PDF in (A.4), the mean and variance of B_n can be derived as:

$$\mathbb{E}\{B_n\} = \frac{\pi\sqrt{L_{\text{IB}}L_{\text{UI}}}}{4}, \tag{A.5}$$

and

$$\mathrm{Var}\left\{B_n\right\} = \left(1 - \frac{\pi^2}{16}\right) L_{\mathrm{IB}} L_{\mathrm{UI}}, \tag{A.6}$$

respectively. Following the approach of [41], we match B_n to Gamma distribution by using the moment-matching approach with $\xi\psi = \mathbb{E}\left\{B_n\right\}$ and $\xi\psi^2 = \mathrm{Var}\left\{B_n\right\}$, where ξ and ψ are the shape and scale parameters of Gamma distribution. For the RV $C = A + \sum_{n=1}^{N} B_n$, the mean and second moment can be expressed as:

$$\mathbb{E}\left\{C\right\} = \frac{\sqrt{\pi L_1}}{2} + N\xi\psi, \tag{A.7}$$

and

$$\mathbb{E}\left\{C^2\right\} = L_1 + N\xi\psi\left(\psi + N\xi\psi + \sqrt{\pi L_1}\right), \tag{A.8}$$

respectively. Then, the variance of C is derived as:

$$\begin{aligned}\mathrm{Var}\left\{C\right\} &= \mathbb{E}\left\{C^2\right\} - \left(\mathbb{E}\left\{C\right\}\right)^2 \\ &= L_1 + N\xi\psi^2 - \frac{\pi L_1}{4}.\end{aligned} \tag{A.9}$$

Again, we match C to Gamma distribution with the corresponding shape and scale parameters given by (11) and (12), respectively. Then, the CDF of $g_1 = C^2$ can be obtained as $F_{g_1}(z) = F_C(\sqrt{z})$ as shown in (10), which completes the proof.

Appendix B: A Proof of Proposition 1

Corresponding to Case II of the RS scheme, the probability $P_{\mathrm{out}}^{(\mathrm{II})}$ can be rewritten as

$$\begin{aligned}P_{\mathrm{out}}^{(\mathrm{II})} &= \Pr\left(g_1 > \eta_1, g_2 > \frac{\rho_1\varepsilon_1^{-1}g_1 - 1}{\rho_2}, \right. \\ &\qquad \left. g_2 < \frac{(1+\varepsilon_1)(1+\varepsilon_2) - (1+\rho_1 g_1)}{\rho_2}\right) \\ &= \mathop{\mathbb{E}}_{\eta_1 < g_1 < \eta_1(1+\varepsilon_2) + \frac{\varepsilon_2}{\rho_1}} \left\{S\right\},\end{aligned} \tag{B.1}$$

where S is defined as

$$\begin{aligned}S \triangleq \Pr\Big(&g_2 > \tfrac{\rho_1\varepsilon_1^{-1}g_1 - 1}{\rho_2} \\ &g_2 < \tfrac{(1+\varepsilon_1)(1+\varepsilon_2) - (1+\rho_1 g_1)}{\rho_2}\Big).\end{aligned} \tag{B.2}$$

Since g_2 is positive in practice, the inequality $\frac{(1+\varepsilon_1)(1+\varepsilon_2)-(1+\rho_1 g_1)}{\rho_2} > 0$ holds true for (B.1), which results in the constraint $g_1 < \eta_1(1+\varepsilon_2) + \frac{\varepsilon_2}{\rho_1}$ for the expectation in (B.1). For the expression of S in (B.2), the upper bound on g_2 should be larger than the lower bound on g_2, which results in the following hidden constraint

$$g_1 < \eta_1(1+\varepsilon_2). \tag{B.3}$$

Therefore, the expectation for S in (B.1) should be taken over $\frac{\rho_1\varepsilon_1^{-1}g_1 - 1}{\rho_2} < g_2 < \frac{(1+\varepsilon_1)(1+\varepsilon_2)-(1+\rho_1 g_1)}{\rho_2}$ and $P_{\mathrm{out}}^{(\mathrm{II})}$ can be given by

$$\begin{aligned}P_{\mathrm{out}}^{(\mathrm{II})} &= \int_{\eta_1}^{\eta_1(1+\varepsilon_2)} \left(F_{g_2}(z_2) - F_{g_2}(z_1)\right) f_{g_1}(y)\, dy \\ &= \int_{\eta_1}^{\eta_1(1+\varepsilon_2)} \left(1 - e^{-\frac{z_2}{L_2}}\right) f_{g_1}(y)\, dy \\ &\quad - \int_{\eta_1}^{\eta_1(1+\varepsilon_2)} \left(1 - e^{-\frac{z_1}{L_2}}\right) f_{g_1}(y)\, dy \\ &= \int_{\eta_1}^{\eta_1(1+\varepsilon_2)} e^{-\frac{z_1}{L_2}} \frac{y^{\frac{k}{2}-1}}{2\theta^k\Gamma(k)} dy \\ &\quad - \int_{\eta_1}^{\eta_1(1+\varepsilon_2)} e^{-\frac{z_2}{L_2}} \frac{y^{\frac{k}{2}-1}}{2\theta^k\Gamma(k)} dy \\ &= \underbrace{\frac{(L_2\rho_2\eta_1)^{\frac{k}{2}}}{2\theta^k\Gamma(k)} \int_0^{\frac{\varepsilon_2}{L_2\rho_2}} \left(x + \frac{1}{L_2\rho_2}\right)^{\frac{k}{2}-1} e^{-x} dx}_{I_1} \\ &\quad \underbrace{- \frac{e^{-\frac{\varepsilon_1+\varepsilon_2+\varepsilon_1\varepsilon_2-\rho_1\eta_1(1+\varepsilon_2)}{\rho_2 L_2}}}{2\theta^k\Gamma(k)} \left(-\frac{\rho_2 L_2}{\rho_1}\right)^{\frac{k}{2}}}_{} \\ &\quad \underbrace{\times \int_0^{\frac{\rho_1\eta_1\varepsilon_2}{\rho_2 L_2}} \left(x - \frac{\rho_1\eta_1(1+\varepsilon_2)}{\rho_2 L_2}\right)^{\frac{k}{2}-1} e^{-x} dx}_{I_2},\end{aligned} \tag{B.4}$$

where $z_1 = \frac{\rho_1\varepsilon_1^{-1}y - 1}{\rho_2}$ and $z_2 = \frac{(1+\varepsilon_1)(1+\varepsilon_2)-(1+\rho_1 y)}{\rho_2}$. By using [40, Eq. (3.382.5)], I_1 and I_2 can be derived as (20) and (21), respectively.

Appendix C: A Proof of Proposition 2

Corresponding to Case I of the RS scheme, the probability $P_{\mathrm{out}}^{(\mathrm{I})}$ can be evaluated as:

$$\begin{aligned}P_{\mathrm{out}}^{(\mathrm{I})} &= \Pr\left(\tau > 0, \rho_2 g_2 \le \tau, R^{(\mathrm{I})} < \hat{R}_2\right) \\ &= \Pr\left(\frac{\rho_1 g_1}{\varepsilon_1} - 1 > 0, \rho_2 g_2 < \min\left\{\frac{\rho_1 g_1}{\varepsilon_1} - 1, \varepsilon_2\right\}\right) \\ &= \Pr\left(0 < \frac{\rho_1 g_1}{\varepsilon_1} - 1 < \varepsilon_2, \rho_2 g_2 < \frac{\rho_1 g_1}{\varepsilon_1} - 1\right) \\ &\quad + \Pr\left(\frac{\rho_1 g_1}{\varepsilon_1} - 1 > \varepsilon_2, \rho_2 g_2 < \varepsilon_2\right) \\ &= \int_{\eta_1}^{\eta_1(1+\varepsilon_2)} F_{g_2}\left(\frac{\rho_1 y}{\rho_2\varepsilon_1} - \frac{1}{\rho_2}\right) f_{g_1}(y)\, dy \\ &\quad + \int_{\eta_1(1+\varepsilon_2)}^{\infty} F_{g_2}\left(\frac{\varepsilon_2}{\rho_2}\right) f_{g_1}(y)\, dy \\ &= F_{g_1}(\eta_1(1+\varepsilon_2))(1 - F_{g_2}(\eta_2)) + F_{g_2}(\eta_2) - F_{g_1}(\eta_1) \\ &\quad - \frac{e^{\frac{1}{\rho_2 L_2}}}{2\theta^k\Gamma(k)} \int_{\eta_1}^{\eta_1(1+\varepsilon_2)} e^{-\frac{\rho_1 y}{\rho_2\varepsilon_1 L_2}} y^{\frac{k}{2}-1} dy \\ &= F_{g_1}(\eta_1(1+\varepsilon_2))(1 - F_{g_2}(\eta_2)) + F_{g_2}(\eta_2) - F_{g_1}(\eta_1) \\ &\quad \underbrace{- \frac{(\rho_2 L_2\eta_1)^{\frac{k}{2}}}{2\theta^k\Gamma(k)} \int_0^{\frac{\varepsilon_2}{\rho_2 L_2}} \left(z + \frac{1}{\rho_2 L_2}\right)^{\frac{k}{2}-1} e^{-x} dx}_{I_3}.\end{aligned} \tag{C.1}$$

By using [40, Eq. (3.382.5)], I_3 can be derived as (24).

Corresponding to Case III of the RS scheme, the probability $P_{\mathrm{out}}^{(\mathrm{III})}$ can be evaluated as:

$$P_{\mathrm{out}}^{(\mathrm{III})} = \Pr\left(\tau = 0, R^{(\mathrm{III})} < \hat{R}_2\right)$$

$$= \Pr\left(0 < g_1 < \eta_1, 0 < g_2 < \frac{(\rho_1 g_1 + 1)\,\varepsilon_2}{\rho_2}\right)$$
$$= \int_0^{\eta_1} \left(F_{g_2}\left(\frac{(\rho_1 y + 1)\,\varepsilon_2}{\rho_2}\right)\right) f_{g_1}(y)\,dy$$
$$= F_{g_1}(\eta_1) - \underbrace{\frac{e^{-\frac{\varepsilon_2}{\rho_2 L_2}}}{2\theta^k \Gamma(k)} \int_0^{\eta_1} e^{-\frac{\rho_1 \varepsilon_2 y}{\rho_2 L_2}} y^{\frac{k}{2}-1} dy}_{I_4}, \quad \text{(C.2)}$$

where I_4 is characterized by the lower incomplete gamma function as shown in (25).

REFERENCES

[1] O. Maraqa, A. S. Rajasekaran, S. Al-Ahmadi, H. Yanikomeroglu, and S. M. Sait, "A survey of rate-optimal power domain NOMA with enabling technologies of future wireless networks," *IEEE Commun. Surveys Tuts.*, vol. 22, no. 4, pp. 2192–2235, Aug. 2020.

[2] Y. Zhang, J. Mu, and J. Xiaojun, "Performance of multi-cell mmwave NOMA networks with base station cooperation," *IEEE Commun. Lett.*, vol. 25, no. 2, pp. 442–445, Oct. 2021.

[3] W. Chen, *et al*., "Backscatter cooperation in NOMA communications systems," *IEEE Trans. Wireless Commun.*, vol. 20, no. 6, pp. 3458–3474, Jan. 2021.

[4] M. W. Akhtar, S. A. Hassan, S. Saleem, and H. Jung, "STBC-aided cooperative NOMA with timing offsets, imperfect successive interference cancellation, and imperfect channel state information," *IEEE Trans. Veh. Technol.*, vol. 69, no. 10, pp. 11712–11727, Aug. 2020.

[5] Y. Sun, Z. Ding, X. Dai, and O. A. Dobre, "On the performance of network NOMA in uplink CoMP systems: A stochastic geometry approach," *IEEE Trans. Commun.*, vol. 67, no. 7, pp. 5084–5098, Mar. 2019.

[6] S. Mounchili and S. Hamouda, "Pairing distance resolution and power control for massive connectivity improvement in NOMA systems," *IEEE Trans. Veh. Technol.*, vol. 69, no. 4, pp. 4093–4103, Feb. 2020.

[7] Z. Ding, P. Fan, and H. V. Poor, "Impact of user pairing on 5G nonorthogonal multiple-access downlink transmissions," *IEEE Trans. Veh. Technol.*, vol. 65, no. 8, pp. 6010–6023, Aug. 2016.

[8] Z. Ding, R. Schober, P. Fan, and H. V. Poor, "Simple semi-grant-free transmission strategies assisted by non-orthogonal multiple access," *IEEE Trans. Commun.*, vol. 67, no. 6, pp. 4464–4478, 2019.

[9] Z. Ding, R. Schober, and H. V. Poor, "Unveiling the importance of SIC in NOMA systems—Part I: State of the art and recent findings," *IEEE Commun. Lett.*, vol. 24, no. 11, pp. 2378–2382, Nov. 2020.

[10] Z. Ding, R. Schober, and H. V. Poor, "A new QoS-guarantee strategy for NOMA assisted semi-grant-free transmission," *IEEE Trans. Commun.*, vol. 69, no. 11, pp. 7489–7503, 2021.

[11] Y. Sun, Z. Ding, and X. Dai, "A new design of hybrid SIC for improving transmission robustness in uplink NOMA," *IEEE Trans. Veh. Technol.*, vol. 70, no. 5, pp. 5083–5087, May 2021.

[12] B. Zheng and R. Zhang, "Intelligent reflecting surface-enhanced OFDM: Channel estimation and reflection optimization," *IEEE Wireless Commun. Lett.*, vol. 9, no. 4, pp. 518–522, 2020.

[13] C. You, B. Zheng, and R. Zhang, "Wireless communication via double IRS: Channel estimation and passive beamforming designs," *IEEE Wireless Commun. Lett.*, vol. 10, no. 2, pp. 431–435, Oct. 2021.

[14] S. Zhang and R. Zhang, "Intelligent reflecting surface aided multi-user communication: Capacity region and deployment strategy," *IEEE Trans. Commun.*, vol. 69, no. 9, pp. 5790–5806, May 2021.

[15] B. Zheng, C. You, and R. Zhang, "Efficient channel estimation for double-IRS aided multi-user MIMO system," *IEEE Trans. Commun.*, vol. 69, no. 6, pp. 3818–3832, Mar. 2021.

[16] J. Zhu, Y. Huang, J. Wang, K. Navaie, and Z. Ding, "Power efficient IRS-assisted NOMA," *IEEE Trans. Commun.*, vol. 69, no. 2, pp. 900–913, Oct. 2021.

[17] X. Mu, Y. Liu, L. Guo, J. Lin, and N. Al-Dhahir, "Exploiting intelligent reflecting surfaces in NOMA networks: Joint beamforming optimization," *IEEE Trans. Wireless Commun.*, vol. 19, no. 10, pp. 6884–6898, Jul. 2020.

[18] A. S. D. Sena, *et al*., "What role do intelligent reflecting surfaces play in multi-antenna non-orthogonal multiple access?" *IEEE Wireless Commun.*, vol. 27, no. 5, pp. 24–31, 2020.

[19] Z. Ding, R. Schober, and H. V. Poor, "On the impact of phase shifting designs on IRS-NOMA," *IEEE Wireless Commun. Lett.*, vol. 9, no. 10, pp. 1596–1600, Apr. 2020.

[20] M. Zeng, X. Li, G. Li, W. Hao, and O. A. Dobre, "Sum rate maximization for IRS-assisted uplink NOMA," *IEEE Commun. Lett.*, vol. 25, no. 1, pp. 234–238, Jan. 2021.

[21] F. Fang, Y. Xu, Q.-V. Pham, and Z. Ding, "Energy-efficient design of IRS-NOMA networks," *IEEE Trans. Veh. Technol.*, vol. 69, no. 11, pp. 14088–14092, Nov. 2020.

[22] Q. Wu and R. Zhang, "Towards smart and reconfigurable environment: Intelligent reflecting surface aided wireless network," *IEEE Commun. Mag.*, vol. 58, no. 1, pp. 106–112, Jan. 2020.

[23] L. Lv, *et al*., "Achieving covert communication by IRS-NOMA," in *Proc. IEEE/CIC ICCC*, 2021, pp. 421–426.

[24] C. Huang, A. Zappone, G. C. Alexandropoulos, M. Debbah, and C. Yuen, "Reconfigurable intelligent surfaces for energy efficiency in wireless communication," *IEEE Trans. Wireless Commun.*, vol. 18, no. 8, pp. 4157–4170, Aug. 2019.

[25] Z. Chen and B. Liu, "Switching signal decoding order in uplink NOMA system with imperfect SIC," *IEEE Commun. Lett.*, vol. 25, no. 11, pp. 3528–3532, Nov. 2021.

[26] Z. Xiang, X. Tong, and Y. Cai, "Secure transmission for NOMA systems with imperfect SIC," *China Commun.*, vol. 17, no. 11, pp. 67–78, 2020.

[27] J. Kim, J. Kim, and S.-H. Park, "Joint design of power control and SIC decoding order for max-min fairness optimization in uplink NOMA systems," in *Proc. ICOIN*, 2021, pp. 339–342.

[28] S. Rezvani, E. A. Jorswieck, N. Mokari, and M. R. Javan, "Optimal versus CSI-based SIC ordering in downlink multi-cell NOMA systems," in *Proc. ICC*, 2021, pp. 1–6.

[29] Y. Mao, *et al*., "Rate-splitting multiple access: Fundamentals, survey, and future research trends," *CoRR*, vol. abs/2201.03192, 2022. [Online]. Available: https://arxiv.org/abs/2201.03192

[30] A. Mishra, Y. Mao, O. Dizdar, and B. Clerckx, "Rate-splitting multiple access for 6G – Part I: Principles, applications and future works," *CoRR*, vol. abs/2205.02548, 2022. [Online]. Available: https://arxiv.org/abs/2205.02548

[31] B. Clerckx, H. Joudeh, C. Hao, M. Dai, and B. Rassouli, "Rate splitting for MIMO wireless networks: A promising PHY-layer strategy for LTE evolution," *IEEE Commun. Mag.*, vol. 54, no. 5, pp. 98–105, May 2016.

[32] Z. Yang, M. Chen, W. Saad, W. Xu, and M. Shikh-Bahaei, "Sum-rate maximization of uplink rate splitting multiple access (RSMA) communication," *IEEE Trans. Mobile Comput.*, vol. 21, no. 7, pp. 2596–2609, 2022.

[33] Y. Zhu, Z. Zhang, X. Wang, and X. Liang, "A low-complexity non-orthogonal multiple access system based on rate splitting," in *Proc. WCSP*, 2017, pp. 1–6.

[34] Y. Zhu, X. Wang, Z. Zhang, X. Chen, and Y. Chen, "A rate-splitting non-orthogonal multiple access scheme for uplink transmission," in *Proc. WCSP*, 2017, pp. 1–6.

[35] J. Zeng, *et al*., "Ensuring max-min fairness of UL SIMO-NOMA: A rate splitting approach," *IEEE Trans. Veh. Technol.*, vol. 68, no. 11, pp. 11080–11093, Nov. 2019.

[36] H. Liu, T. A. Tsiftsis, K. J. Kim, K. S. Kwak, and H. V. Poor, "Rate splitting for uplink NOMA with enhanced fairness and outage performance," *IEEE Trans. Wireless Commun.*, vol. 19, no. 7, pp. 4657–4670, Jul. 2020.

[37] H. Liu, *et al*., "A new rate splitting strategy for uplink CR-NOMA systems," *IEEE Trans. Veh. Technol.*, vol. 71, no. 7, pp. 7947–7951, 2022.

[38] H. Liu, Y. Ye, Z. Bai, K. J. Kim, and T. Tsiftsis, "Rate splitting multiple access aided mobile edge computing in cognitive radio networks," in *Proc. IEEE ICC Workshops*, 2022, pp. 1–5.

[39] B. Rimoldi and R. Urbanke, "A rate-splitting approach to the Gaussian multiple-access channel," *IEEE Trans. Inf. Theory*, vol. 42, no. 2, pp. 364–375, Mar. 1996.

[40] I. S. Gradshteyn and I. M. Ryzhik, "Table of integrals, series, and products," *Mathematics of Computation*, vol. 20, no. 96, p. 1157–1160, 2007.

[41] T. Van Chien, L. T. Tu, S. Chatzinotas, and B. Ottersten, "Coverage probability and ergodic capacity of intelligent reflecting surface-enhanced communication systems," *IEEE Commun. Lett.*, vol. 25, no. 1, pp. 69–73

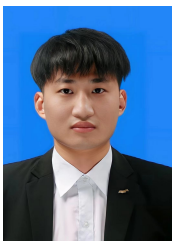

Haoyu You received the BS degree in Electrical Engineering from Anhui Sanlian University, Hefei, China, in 2018. He is currently pursuing the MS degree in Shandong Jiaotong University. His research interests include cognitive radios and cooperative communications.

Zhiquan Bai (Member, IEEE) received the M.Eng. degree in Communication and Information System from Shandong University, Jinan, China, in 2003, and the Ph.D. degree (Hons.) from INHA University, Incheon, South Korea, in 2007, under the Grant of Korean Government IT Scholarship. He held a Postdoctoral position with INHA University, and was a Visiting Professor with The University of British Columbia, Canada. He is currently an Associate Professor with the School of Information Science and Engineering, Shandong University. His research interests include cooperative technology and spatial modulation, MIMO technology, VLC, resource allocation and optimization, and deep-learning-based 5G wireless communications. He is an Associate Editor of the International Journal of Communication Systems.

Hongwu Liu (Senior Member, IEEE) received the Ph.D. degree from Southwest Jiaotong University in 2008. From 2008 to 2010, he was with Nanchang Hangkong University. From 2010 to 2011, he was a Post-Doctoral Fellow with the Shanghai Institute of Microsystem and Information Technology, Chinese Academy of Science. From 2011 to 2013, he was a Research Fellow with the UWB Wireless Communications Research Center, Inha University, South Korea. Since 2014, he has been an Associate Professor with Shandong Jiaotong University. From 2017 to 2018, he was a Research Professor with the Department of Information and Communication Engineering, Inha University. His research interests include MIMO signal processing, cognitive radios, cooperative communications, wireless secrecy communications, and AI-based wireless communications.

Theodoros A. Tsiftsis (Senior Member, IEEE) was born in Lamia, Greece, in 1970. He received the BSc degree in physics from the Aristotle University of Thessaloniki, Greece, in 1993, the MSc degree in Digital Systems Engineering from the Heriot-Watt University, Edinburgh, U.K., in 1995, the MSc degree in Decision Sciences from the Athens University of Economics and Business, in 2000, and the PhD degree in Electrical Engineering from the University of Patras, Greece, in 2006. He is currently a Professor in the School of Intelligent Systems Science & Engineering at Jinan University, Zhuhai, China, and also Honorary Professor at Shandong Jiaotong University, Jinan, China.

His research interests include the broad areas of cognitive radio, communication theory, wireless powered communication systems, optical wireless communication, and ultra-reliable low-latency communication. He has served as Senior or Associate Editor in the Editorial Boards of IEEE TRANSACTIONS ON VEHICULAR TECHNOLOGY, IEEE COMMUNICATIONS LETTERS, IET COMMUNICATIONS, and IEICE TRANSACTIONS ON COMMUNICATIONS. He is currently an Area Editor for Wireless Communications II of the IEEE TRANSACTIONS ON COMMUNICATIONS and an Associate Editor of the IEEE TRANSACTIONS ON MOBILE COMPUTING. Prof. Tsiftsis has been appointed to a 2-year term as an IEEE Vehicular Technology Society Distinguished Lecturer (IEEE VTS DL), Class 2018.

Kyung Sup Kwak (Member, IEEE) received the Ph.D. degree from the University of California at San Diego and worked for Hughes Network Systems and IBM Network Analysis Center, USA. Since then, he has been with the School of Information and Communication Engineering, Inha University, South Korea as a Professor and served as the Dean of the Graduate School of Information Technology and Telecommunications and the Director of UWB Wireless Communications Research Center, a IT research center, South Korea, since 2003. In 2006, he served as the president of Korean Institute of Communication Sciences (KICS), and in 2009, the president of Korea Institute of Intelligent Transport Systems (KITS). His research interests include multiple access communication systems, mobile and UWB radio systems, future IoT, and wireless body area networks: nano networks and molecular communications. In 1993, he received the Engineering College Achievement Award from Inha University and a service award from the Institute of Electronics Engineers of Korea. In 1996 and 1999, he received distinguished service awards from the KICS. He received the LG Paper Award in 1998 and Motorola Paper Award in 2000. He received Official Commendations for UWB radio technology research and development from the Minister of Information and Communication, Prime Minister, and President of Korea in 2005, 2006, and 2009, respectively. In 2007, he received Haedong Paper Award and in 2009, Haedong Scientific Award of research achievement. In 2008, he was elected as an Inha Fellow Professor and currently as an Inha Hanlim Fellow Professor.